AGU PUBLICATIONS

JGR

Journal of Geophysical Research: Oceans

RESEARCH ARTICLE

10.1002/2013JC009579

Key Points:
- The annual Bering Sea CO_2 sink is ~6.8 Tg C yr^{-1}
- Autumn and winter effluxes balanced ~65% of spring and summer influxes
- Ice cover limited fluxes by enhancing cooling and slowing wind speeds

Supporting Information:
- Readme
- Figure S1
- Figure S2
- Figure S3

Correspondence to:
J. N. Cross,
jessica.cross@noaa.gov

Citation:
Cross, J. N., J. T. Mathis, K. E. Frey, C. E. Cosca, S. L. Danielson, N. R. Bates, R. A. Feely, T. Takahashi, and W. Evans (2014), Annual sea-air CO_2 fluxes in the Bering Sea: Insights from new autumn and winter observations of a seasonally ice-covered continental shelf, *J. Geophys. Res. Oceans*, *119*, 6693–6708, doi:10.1002/2013JC009579.

Received 4 NOV 2013
Accepted 28 AUG 2014
Accepted article online 2 SEP 2014
Published online 9 OCT 2014

Annual sea-air CO_2 fluxes in the Bering Sea: Insights from new autumn and winter observations of a seasonally ice-covered continental shelf

Jessica N. Cross[1,2], Jeremy T. Mathis[1,2], Karen E. Frey[3], Catherine E. Cosca[1], Seth L. Danielson[2], Nicholas R. Bates[4], Richard A. Feely[1], Taro Takahashi[5], and Wiley Evans[1,2]

[1]National Oceanic and Atmospheric Administration, Pacific Marine Environmental Laboratory, Seattle, Washington, USA, [2]Ocean Acidification Research Center, University of Alaska, Fairbanks, Fairbanks, Alaska, USA, [3]Graduate School of Geography, Clark University, Worcester, Massachusetts, USA, [4]Bermuda Institute of Ocean Sciences, St. Georges, Bermuda, [5]Lamont-Doherty Earth Observatory, Palisades, New York, USA

Abstract High-resolution data collected from several programs have greatly increased the spatiotemporal resolution of pCO_2(sw) data in the Bering Sea, and provided the first autumn and winter observations. Using data from 2008 to 2012, monthly climatologies of sea-air CO_2 fluxes for the Bering Sea shelf area from April to December were calculated, and contributions of physical and biological processes to observed monthly sea-air pCO_2 gradients (ΔpCO_2) were investigated. Net efflux of CO_2 was observed during November, December, and April, despite the impact of sea surface cooling on ΔpCO_2. Although the Bering Sea was believed to be a moderate to strong atmospheric CO_2 sink, we found that autumn and winter CO_2 effluxes balanced 65% of spring and summer CO_2 uptake. Ice cover reduced sea-air CO_2 fluxes in December, April, and May. Our estimate for ice-cover corrected fluxes suggests the mechanical inhibition of CO_2 flux by sea-ice cover has only a small impact on the annual scale (<2%). An important data gap still exists for January to March, the period of peak ice cover and the highest expected retardation of the fluxes. By interpolating between December and April using assumptions of the described autumn and winter conditions, we estimate the Bering Sea shelf area is an annual CO_2 sink of ~6.8 Tg C yr^{-1}. With changing climate, we expect warming sea surface temperatures, reduced ice cover, and greater wind speeds with enhanced gas exchange to decrease the size of this CO_2 sink by augmenting conditions favorable for greater wintertime outgassing.

1. Introduction

The largest annual advance and retreat of seasonal sea ice in high-latitude marginal seas occurs over the Bering Sea shelf (~1700 km latitudinally) [*Walsh and Johnson*, 1979]. This annual sea ice cycle creates differing physical regimes across the northern and southern regions of the continental shelf [*Stabeno et al.*, 2002, 2012a]. Ice-affected waters exhibit colder temperatures, a differing pycnocline, and clear marine ecosystem differences compared to the ice-free areas of the southern shelf [e.g., *Stabeno et al.*, 2012a]. Whereas the impact of sea ice on shaping the spring and summer physical environments and ecosystems of the Bering Sea shelf is well known [*Stabeno et al.*, 2010; *Cooper et al.*, 2013; *Hunt et al.*, 2002; *Hunt et al.*, 2011], seasonal ice cover presents logistical and financial challenges that have limited data collection during autumn and winter.

As a result, a broad range of estimates of sea-air CO_2 fluxes are available for the Bering Sea, with a variety of different approaches used to extrapolate sea-air fluxes to periods without data. Extrapolation techniques that use models, data syntheses, and climatological approaches mask small-scale variability and result in annual fluxes on the order of 10 Tg C yr^{-1} [*Walsh and Dieterle*, 1994; *Chen and Borges*, 2009]. Annual estimates derived strictly from the extrapolation of observational data overemphasize the extremely rapid rates of exchange observed during blooms, and can be a full order of magnitude higher (on the order of 100–200 Tg C yr^{-1}) [*Bates et al.*, 2011; *Chen et al.*, 2004]. All of these approaches utilize data collected only during spring and summer. Because wintertime data are unavailable, fluxes occurring during this period are typically ignored under the assumption that ice cover causes complete mechanical inhibition of gas exchange [*Bates et al.*, 2011], although spatially and temporally variable ice cover [*Stabeno et al.*, 2012b] could provide ample opportunities for these exchanges to occur. Furthermore, these potential fluxes could be quite large.

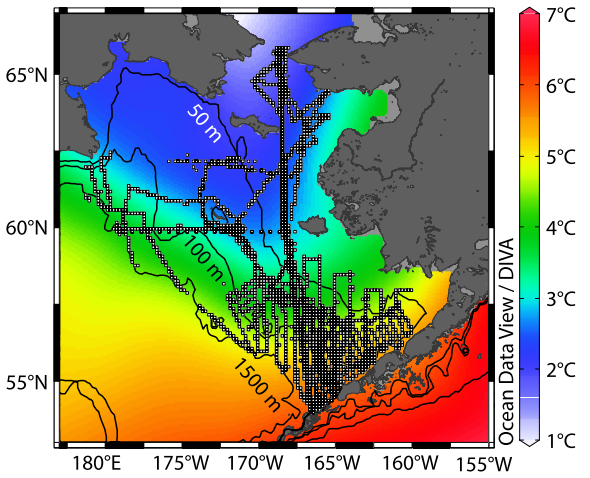

Figure 1. Map of the southeastern Bering Sea shelf. Color shading indicates the 5 year (2008–2012) mean annual sea surface temperature. Data are taken from the Extended Reconstructed Sea Surface Temperature (ERSST) data available at http://www.ncdc.noaa.gov/ersst/. Also shown are populated grid cells (white squares) and the location of the M2 mooring (X). Image was created using Ocean Data View [R. Schlitzer, 2014] (http://odv.awi.de).

The Bering Sea is among the most productive ecosystems in the global oceans, and previous studies of the carbon cycle have shown strong efficiency of the biological pump over the shallow shelf. Respiration and storage of this carbon occurs in bottom waters during summer, but can easily be returned to the surface by vertical overturning induced by the onset of the late summer and autumn storm season. CO_2 accumulation at the surface layer from this respiration signal combined with enhanced exchange rates that have been reported during periods of ice formation [*Else et al*., 2011; *Miller et al*., 2011] could result in rapid outgassing. Strong effluxes could also occur during with the onset of ice melt during late winter and early spring. Other studies in Alaskan coastal waters have shown that CO_2 produced by late-season respiration processes accumulates in ice-covered waters [*Semiletov*, 1999; *Semiletov et al*., 2004], potentially resulting in rapid outgassing upon ice retreat. CO_2 effluxes occurring during this previously neglected winter period could result in a substantial decrease of the Bering Sea sink for atmospheric CO_2.

Recently, the spatiotemporal resolution of data for the entire Bering Sea shelf has significantly improved through the collection of new in-situ sea surface CO_2 partial pressure (pCO_2(sw)) data from underway flow-through systems on several vessels, along with over a dozen large-scale repeat hydrography surveys and the first deployment of moored autonomous carbon sensors in the region (Figure 1) [*Mathis et al*., 2014]. These data included of pCO_2(sw) during autumn and winter, providing the unique opportunity to examine the potential contributions of respiration and sea ice formation to CO_2 fluxes in this dynamic area. Here we synthesized surface seawater data collected during 21 cruises over a 5 year period with reconstructed atmospheric pCO_2 (pCO_2(atm)), climatological winds, and passive microwave-derived sea ice concentration data to generate a monthly climatology of sea-air CO_2 fluxes (ΔpCO_2) between April and December. This approach quantifies sea-air CO_2 flux at high spatial resolution ($\sim$12 km^2), reduces temporal extrapolation errors by including the first autumn and winter observations, and scales the impact of autumn and winter respiration and the contribution of sea ice for the first time in this geographic region.

2. Methods

An expansive data set of pCO_2(sw) (μatm) was compiled from a variety of sources, with over 45,000 measurements spanning the 5 year period from 2008 to 2012 (Figure 1 and Table 1), including: (1) continuous direct measurements of pCO_2(sw) from underway systems obtained aboard the USCGC *Healy* by the Lamont Doherty Earth Observatory (LDEO) Carbon Group (data available at http://www.ldeo.columbia.edu/res/pi/CO2/ and at the Carbon Dioxide Information and Analysis Center (CDIAC), *Takahashi et al*. [2014]), and by the National Oceanic and Atmospheric Administration (NOAA) aboard the NOAA Ship *Oscar Dyson* (available from the Pacific Marine Environmental Laboratory data portal (http://www.epic.noaa.gov/ewb); (2) a continuous 5 month record from May to October 2011 of autonomously collected pCO_2(sw) data from the M2 mooring site by NOAA [*Mathis et al*., 2014]; (3) pCO_2(sw) data calculated from previously published discrete dissolved inorganic carbon (DIC) and total alkalinity (TA) samples collected during the Bering Sea Project (2008–2010; bsierp.nprb.org) [*Bates et al*., 2011; *Mathis et al*., 2011a, 2011b; *Cross et al*., 2012, 2013]. pCO_2(sw) was calculated from DIC and TA measurements and associated hydrographic data [*Zeebe and Wolf-Gladrow*, 2001; *Dickson et al*., 2007] using CO2SYS version 1.05 using the thermodynamic model of

Table 1. Data Sets Included in This Synthesis, Including the Cruise Title or Data Set Title, Contributor, Period of Record, Types of pCO_2(sw) Measurements Collected, and the Number of Measurements From the Data Record Included in the Bounds of the Bering Sea Shelf in This Synthesis Work (*n*)

Cruise	Contributor	Period of Record	Type	*n*
HLY0802	BEST	1 Apr 2008 to 5 May 2008	Calc. from Obs.	57
HLY0803	BEST	5 Jul 2008 to 29 Jul 2008	Calc. from Obs.	72
HLY0902	BEST	4 Apr 2009 to 10 May 2009	Calc. from Obs.	58
KN195	BEST	22 Jun 2009 to 12 Jul 2009	Calc. from Obs.	68
MF0904	BEST	26 Sep 2009 to 9 Oct 2009	Calc. from Obs.	58
TN249	BEST	14 May 2010 to 11 Jun 2010	Calc. from Obs.	36
TN250	BEST	24 Jun 2010 to 12 Jul 2010	Calc. from Obs.	63
M2	NOAA	20 May 2011 to 26 Sep 2011	Mooring	990
DY1101	NOAA	18 May 2011 to 28 May 2011	Underway	4231
DY1102	NOAA	31 May 2011 to 1 Jun 2011	Underway	146
DY1204	NOAA	29 Apr 2012 to 3 May 2012	Underway	2060
DY1205_06	NOAA	16 May 2012 to 2 Jun 2012	Underway	5222
DY1207_L1	NOAA	12 Jun 2012 to 25 Jun 2012	Underway	5565
DY1207_L3	NOAA	4 Aug 2012 to 10 Aug 2012	Underway	2731
DY1208_L1	NOAA	21 Aug 2012 to 2 Sep 2012	Underway	5527
HLY1102	LDEO	20 Jun 2011 to 26 Jul 2011	Underway	2981
HLY1103	LDEO	24 Sep 2011 to 27 Sep 2011	Underway	1265
HLY1104	LDEO	02 Oct 2011 to 26 Oct 2011	Underway	2196
HLY1105	LDEO	10 Nov 2011 to 15 Dec 2011	Underway	9183
HLY1202	LDEO	12 Aug 2012 to 27 Sep 2012	Underway	1504
HLY1203	LDEO	5 Oct 2012 to 24 Oct 2012	Underway	2035

Robbins et al. [2010] as updated from *Lewis and Wallace* [1998], the borate dissociation constant of *Dickson* [1990], the silicate and phosphate dissociation constants listed by *Dickson et al*. [2007], the carbonic acid dissociation constants of *Dickson and Millero* [1987] as updated from *Mehrbach et al*. [1973], and the CO_2 solubility equations of *Weiss* [1974].

pCO_2(sw) data were extracted from these cruises for the area of the Bering Sea shelf, bounded by the Aleutian Islands, Bering Strait (65.88°N), the Alaskan coastline, and the 1500 m isobath, which is a standard proxy for the Bering Sea shelf break. These data were combined with a time/space colocated atmospheric pCO_2 product (μatm) described in detail by *Evans and Mathis* [2013] to calculate sea-minus-air pCO_2 differences (ΔpCO_2; μatm). This treatment implicitly captures secular increases in both seawater and atmospheric pCO_2 [*Evans and Mathis*, 2013]. CO_2 solubility (K_{CO_2}; mmol m^{-3} atm^{-1}) was calculated from ancillary measurements of sea surface temperature (SST; °C) and sea surface salinity (SSS) using the relationship from *Weiss* [1974] corrected for seawater density. Following the approach of *Evans et al*. [2013] and *Evans and Mathis* [2013], ΔpCO_2, SST, SSS, and CO_2 solubility data were averaged within 0.1° latitude by 0.2° longitude grid cells, creating monthly climatologies of each parameter.

These climatologies were coupled with monthly averaged piston velocities (k_{SST}; m d^{-1}) to calculate fluxes. Piston velocities were derived from monthly averages of daily second moments of the wind speed, according to the method of *Evans et al*. [2014], using the wind speed parameterization from *Ho et al*. [2011]. Daily second moments of the wind speed were generated from 10 years of daily surface wind speeds (2003–2012) computed from 1000 hPa meridional and zonal wind velocities from the National Centers for Environmental Prediction (NCEP) North American Regional Reanalysis (NARR; available from esrl.noaa.gov; Figure S1 in supporting information). The NARR product is an extension of the NCEP Global Reanalysis (GR2) based on both data and modeled products. These data are provided by the NOAA Earth System Research Laboratory (ESRL) in a Lambert Conformal grid with approximately 32 km resolution, and were interpolated here to a 0.25° latitude by 0.25° longitude uniform grid.

NARR represents an improvement in both accuracy and resolution for the North American regional area over GR2 [*Mesinger et al*., 2006]. Unlike GR2, NARR includes the presence or absence of sea ice as a lower boundary condition for the meteorological model used to calculate wind speeds. Another wind product with similarly high spatial resolution available for the Bering Sea is the Scatterometer Climatology of Ocean Winds (SCOW) used by *Evans and Mathis* [2013]. The northern limit of these data is ~60°N (Figure S2 in supporting information), spanning only half the Bering Sea shelf whereas NARR has complete spatial coverage.

The final result of these calculations is a monthly climatology of sea-air CO_2 fluxes (F_{CO_2}; mmol CO_2 m^{-2} d^{-1}) at 0.1° latitude by 0.2° longitude resolution across the Bering Sea shelf calculated such that:

$$F_{CO_2} = k_{SST} \times K_{CO_2} \times \Delta pCO_2.$$

According to these calculations, negative fluxes indicate transfer of CO_2 into the surface ocean from the atmosphere (influx), while positive fluxes indicate transfer of CO_2 out of the surface ocean and into the atmosphere (efflux).

Recent work has suggested that there can be significant fluxes of CO_2 through ice fields [*Delille et al*., 2007; *Nomura et al*., 2010; *Miller et al*., 2011; *Else et al*., 2008, 2011; *Mucci et al*., 2010; *Rysgaard et al*., 2011], and that some ice-associated waters (e.g., polynyas) can exhibit enhanced gas transfer velocities relative to those computed from typical wind speed parameterizations [e.g., *Else et al*., 2011; *Loose et al*., 2014]. However, many of these results are based on small footprint eddy covariance measurements, and a standard operational method for estimating gas transfer over broad ice-rich environments is currently lacking. In addition, errors associated with eddy covariance in cold marine environments [*Burba et al.,* 2008; *Ono et al.,* 2008; *Prytherch et al.,* 2010; *Lauvset et al.,* 2011; *Landwehr et al.,* 2014] cast some doubt on these results, as discussed by *Else et al.* [2011]. For example, when corrections for CO_2–H_2O cross correlation are applied to eddy covariance measurements, the magnitude of the fluxes calculated from these data are reduced to levels comparable to those that would be computed from bulk formulae [e.g., *Lauvset et al.,* 2011; *Landwehr et al.,* 2014]. Other methods of calculating gas exchange of CO_2 through ice have indicated that exchange rates may be negligible [*Rutgers van der Loeff et al*., 2014].

Given that community agreement on the issues surrounding gas transfer through ice is still evolving (broadly reviewed by *Vancoppenolle et al*. [2013]), it is not presently possible to offer a generic model describing the influence of sea ice on CO_2 fluxes. Instead, we here apply a conservative estimate of the mechanical impact of ice on F_{CO_2} based on monthly ice concentration (C), such that:

$$F_{CO_2 i} = F_{CO_2} \times \frac{100 - C}{100}.$$

In order to account for gas transfer through the ice matrix and gas transfer through small-scale open-water areas generated by continuous ice deformation (leads, polynyas, grain boundaries, and microcracks), grid cells with >90% ice cover were reduced to 90% [*Takahashi et al*., 2009]. This ensured some amount of gas transfer even in the presence of full ice cover. Monthly climatologies of sea ice concentration were derived from daily 12 km^2 resolution gridded Special Sensor Microwave Imager (SSM/I) ice concentration data processed by the National Snow and Ice Data Center (NSIDC) and provided by the French Research Institute for Exploration of the Sea (IFREMER), available through the CERSAT archive (cersat.ifremer.fr; Figure S3 in supporting information).

In order to constrain the influence of changing temperatures on F_{CO_2}, pCO_2(sw) values were normalized to the 2008–2012 mean annual SST from the equation of *Takahashi et al*. [2002], such that $(pCO_2 \ at \ T_{mean}, \ \text{or} \ npCO_2(\text{sw})) = (pCO_2(\text{sw}) \ at \ T_{obs}) \times e^{[0.0423(T_{mean} - T_{obs})]}$. Our mean annual SST was derived from 5 years of annually averaged Extended Reconstructed Sea Surface Temperature (ERSST) data (http://www.ncdc.noaa.gov/ersst/; Figure 1). This calculation removes localized effects of warming and cooling on pCO_2(sw) values, such that the temperature effect at any one time relative to the annual average can be estimated as the difference between pCO_2(sw) and normalized pCO_2 ($npCO_2$(sw)).

Accordingly, the variations in $npCO_2$(sw) should be the result of any additional processes that modify pCO_2(sw) other than changing temperature, such as biological CO_2 utilization, sea-air exchange of CO_2, and vertical/lateral transport of CO_2 and alkalinity. Most studies assume that after temperature normalization, remaining variations in $npCO_2$(sw) are the result of biogeochemical modification [e.g., *Bates et al*., 2011; *Takahashi et al*., 2002], and absorb these other factors as minor sources of error in a biological term. The relative contributions of these other sources of variation in $npCO_2$(sw) are discussed in section 3.5.

In order to represent the impacts of changing temperature (T) and biological processes (B) on CO_2 fluxes, we estimated their contributions to the monthly sea-air pCO_2 gradient and constructed two new monthly climatological parameters, such that:

$$T = \left(pCO_{2(\text{SW})} - pCO_{2(\text{atm})}\right) - \left(npCO_{2(\text{SW})}\right) - pCO_{2(\text{atm})}) = \Delta pCO_2 - n\Delta pCO_2$$

$$B = npCO_{2(\text{SW})} - pCO_{2(\text{atm})} = n\Delta pCO_2$$

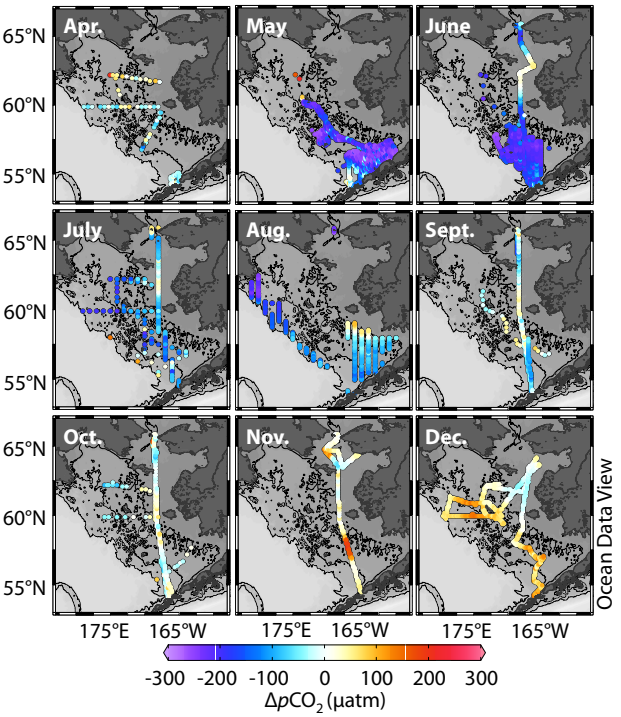

Figure 2. Monthly sea-air ΔpCO_2 values for the Bering Sea shelf (μatm). Warm colors indicate positive gradients (favoring efflux), while cool colors indicate negative gradients (favoring influx). Image was created using Ocean Data View [R. Schlitzer, 2014] (http://odv.awi.de).

These estimates were made at single time points rather than estimated as change through time. An important caveat in this method of differentiating flux drivers is that equilibration with the atmosphere may be slower than the 1 month time scale over which we have averaged sea-air pCO_2 gradients. As a result, monthly estimates of T and B may contain some remnant of forcing generated during the previous months.

Shelf-wide average rates of ΔpCO_2(sw), T, B, F_{CO_2}, and $F_{CO_2 i}$ were area weighted according to the area of each grid cell, such that:

$$Avg(C)_{aw} = \frac{\sum_{i=1}^{n}(C_i \times A_i)}{\sum_{i=1}^{n}(A_i)}$$

where C is the parameter, i is an individual grid cell, A is the grid cell area, and n is the number of grid cells occupied during each month. The positive and negative contributions of B and T, indicating respiration, warming, primary production, and cooling, respectively, were also averaged across the entire shelf and weighted according to the area of each grid cell and the number of positive or negative grid cells in each month ($n_{\pm}$) relative to the total number of occupied grid cells in each month (n_{tot}), such that:

$$Avg(C_{\pm})_{aw} = \frac{\sum_{i=1}^{n_{\pm}}(C_i \times A_i)}{\sum_{i=1}^{n_{\pm}}(A_i)} \times \frac{n_{\pm}}{n_{tot}}.$$

3. Results and Discussion

3.1. Observations

The monthly climatology of ΔpCO_2 shown in Figure 2 reveals periods of both CO_2 oversaturation ($\Delta pCO_2 > 0$; warm colors, Figure 2) and undersaturation ($\Delta pCO_2 < 0$; cool colors, Figure 2). Spatial variability was also apparent during most months. Over the southern shelf (<60°N), ΔpCO_2 values were undersaturated from April to September, although some areas of weak oversaturation (as high as +92 μatm) were evident as early as August particularly in the nearshore environment. Shelf surface waters became oversaturated on average over the southern shelf in December. Data coverage was more sparse and irregular over the northern shelf, especially during April, May, and August. However, available data point toward an offset in the seasonal oscillation of oversaturation and undersaturation relative to the southern shelf. Oversaturation was evident in April and May, while the southern shelf was undersaturated at that time. In December, the coastal northern shelf was mostly undersaturated or near equilibrium with the atmosphere, while the southern shelf and shelf break were oversaturated.

Normalized to the climatological mean temperature (see color shading, Figure 1), spatial patterns in CO_2 oversaturation and undersaturation appeared much more uniform within any given month ($n\Delta pCO_2$, Figure 3). According to our assumption that variations in $n\Delta pCO_2$ indicate the influences of primary productivity and respiration, high rates of primary production decreased $n\Delta pCO_2$ during May, and continued to maintain undersaturations of CO_2 through October. In November, only weakly undersaturated levels of CO_2 remained. During this transition month, $n\Delta pCO_2$ was either close to equilibrium or oversaturated with

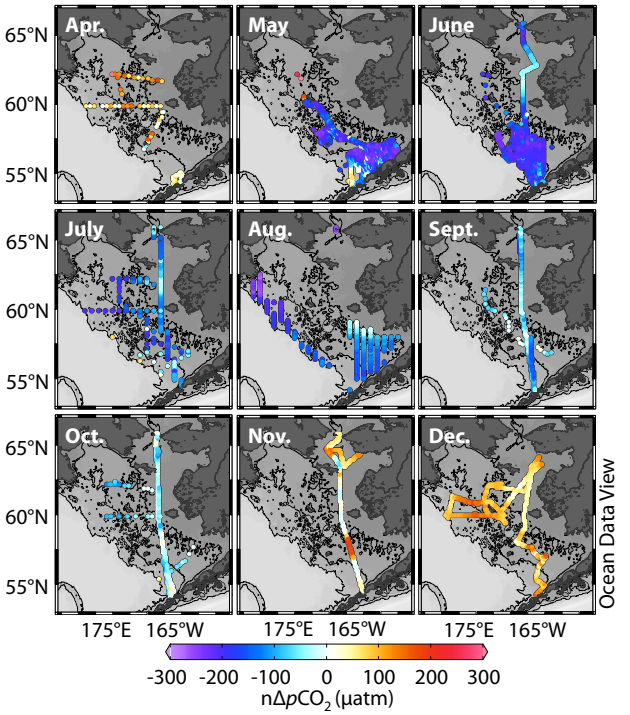

Figure 3. Monthly normalized sea-air ΔpCO_2 values for the Bering Sea shelf ($n\Delta pCO_2$; μatm). Normalization was performed according to the method of *Takahashi et al*. [2002], using the mean annual sea surface temperature shown in Figure 1. The resulting gradients indicate the influence of production and respiration on ΔpCO_2. Image was created using Ocean Data View [R. Schlitzer, 2014] (http://odv.awi.de).

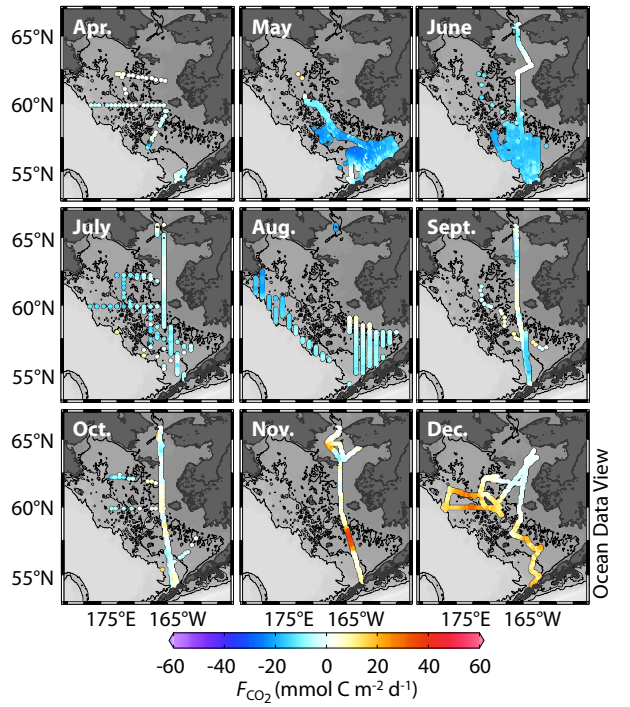

Figure 4. Monthly sea-air CO_2 flux for the Bering Sea shelf (F_{CO_2}; mmol CO_2 m^{-2} d^{-1}). Warm colors indicate net efflux, while cool colors indicate net influx.

respect to the atmosphere, indicating that respiration had begun to balance or surpass rates of primary production on pCO_2(sw). In December and April, oversaturated conditions clearly dominated the entire shelf. The dominant control on *B* transitioned between net heterotrophy and net autotrophy between April and May. In any month, distinct differences in *T* and *B* between the northern and southern regions of the shelf were not apparent or very small.

This spatial homogeneity in *T* and *B*, with most of the shelf exhibiting impacts from either high rates of primary production or respiration, or either warming or cooling, within any 1 month, indicates that the offset in the cycle of net ΔpCO_2 between the northern shelf and the southern shelf was not directly linked to either driver. Instead, the offset is caused by differences in the seasonal cycle of these drivers. Primary productivity began and peaked in May, declining variously through October. However, warming did not substantially impact ΔpCO_2 values until June, and the influence of *T* did not peak until September. The offset in ΔpCO_2 between the northern and southern shelves we observed in April and December results when weakening biogeochemical processes are overwhelmed by strengthening temperature forcing. The balance between these two drivers varies spatially between the northern and southern shelves. Over the central shelf (in the area north of Nunivak Island and southeast of St. Lawrence Island), ΔpCO_2 values are almost always very close to equilibrium due to the opposing forces of biological processes and changing temperature.

As a result of this balanced ΔpCO_2, central shelf F_{CO_2} values were almost always close to zero (Figure 4). However, F_{CO_2} magnitudes were also very small in other areas due to spatially and temporally variable piston velocities. This was particularly prevalent in May, where the lowest piston velocities reached only 0.7 m d^{-1}, and sea-air pCO_2 differences of -254 μatm produced F_{CO_2} of only -11 mmol CO_2 m^{-2} d^{-1} over the northern shelf and southeastern coast. During

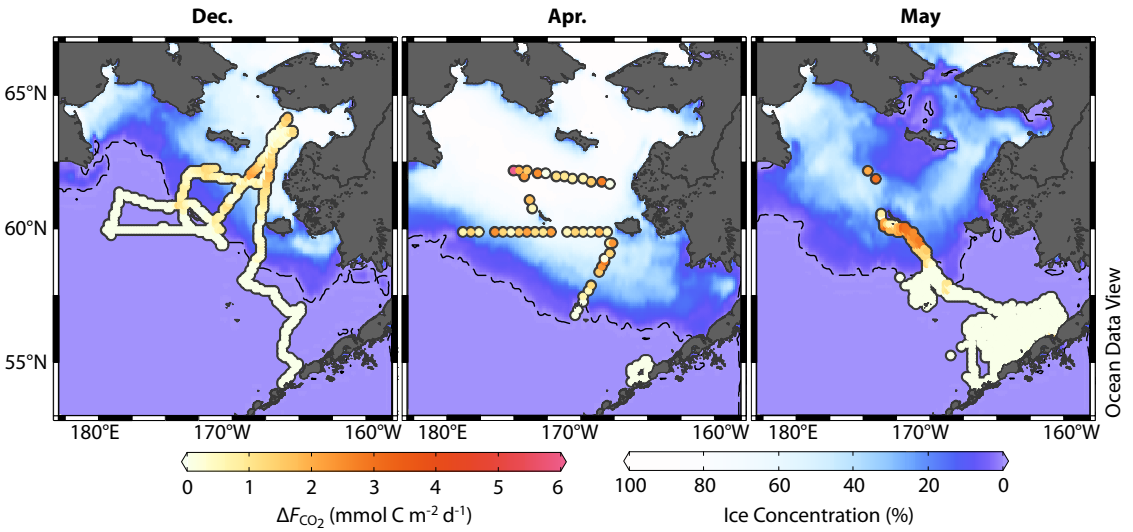

Figure 5. Dampening of F_{CO_2} values caused by the mechanical inhibition of gas exchange by sea ice, according to our parameterization. Because low wind speeds cooccurred with ice cover, potential F_{CO_2} values were very low, and resulting dampening was similarly small. Image was created using Ocean Data View [R. Schlitzer, 2014] (http://odv.awi.de).

the same month, much lower gradients (−99 μatm) coupled with higher piston velocities (1.5 m d^{-1}) produced an equivalent F_{CO_2}. Overall, ΔpCO_2 values were most negative during May (−277 μatm at minimum), but low gas exchange rates resulted in F_{CO_2} only as large as −27 mmol CO_2 m^{-2} d^{-1} at maximum. While ΔpCO_2 values were lower in magnitude during November (+204 μatm), high exchange rates resulted in the largest annual F_{CO_2} (+42 mmol CO_2 m^{-2} d^{-1}).

Low piston velocities were also generally observed over areas with a high sea ice concentration (Figure 5; Figures S1 and S3 in supporting information). The NARR wind product includes the presence/absence sea ice as a lower boundary condition [*Mesinger et al.*, 2006], which influences the parameterizations of surface roughness during the calculation of wind speeds. Because surface roughness is higher over sea ice than over open water, the monthly second moments of the wind speed were reduced in areas of ice cover. As a result, F_{CO_2} values in ice-covered areas were already generally near zero due to the resultant lower piston velocities. This data set spans three ice-affected months: December, April, and May. Applying the conservative dampening estimation we described earlier reduced both influxes and effluxes by only as much as 5 mmol CO_2 m^{-2} d^{-1}. Most ice-affected stations were dampened by <3 mmol CO_2 m^{-2} d^{-1}. Although ice concentrations were lower during May compared to December and April, ΔpCO_2 was also farther departed from equilibrium in May relative to the other ice-affected months. As a result, the maximum magnitudes of mechanical inhibition of F_{CO_2} by sea ice were greatest during May.

3.2. Annual Shelf-Wide Fluxes and the Impacts of Late-Season Drivers

Integrating F_{CO_2} rates over the number of days in each month and area of each grid cell allowed us to determine the area-weighted average monthly flux ($F_{CO_2(aw)}$; Tg C month^{-1}) and the relative drivers of F_{CO_2}, revealing a clear seasonal cycle for the Bering Sea surface waters (Figure 6 and Table 2). The spring and summer trends corresponded well to recent synthesis efforts conducted by the participants in the Bering Ecosystem Study (BEST) Program and Bering Sea Integrated Ecosystem Research Project (BSIERP) [*Stabeno et al.*, 2012a, 2012b; *Sigler et al.*, 2014; *Dornblaser and Striegl*, 2007; *Sigler et al.*, 2014]. $F_{CO_2(aw)}$ peaked in May (−4.10 Tg C month^{-1}) and June (−3.39 Tg C month^{-1}) with the onset of ice ablation, typically associated with rapidly increasing rates of primary production of the spring bloom. After a brief weakening in July (−1.62 Tg C month^{-1}), perhaps caused by nutrient depletion or grazing pressure [*Lomas et al.*, 2012], a secondary peak in $F_{CO_2(aw)}$ was observed in August (−2.33 Tg C month^{-1}), earlier than previously documented autumn blooms [*Sigler et al.*, 2014]. $F_{CO_2(aw)}$ decreased in September (−1.26 Tg C month^{-1}) as the contribution of changing temperature peaked and the influence of biological processes slackened. During October, the impacts of changing temperature and rates of primary production on ΔpCO_2 were nearly equivalent (32

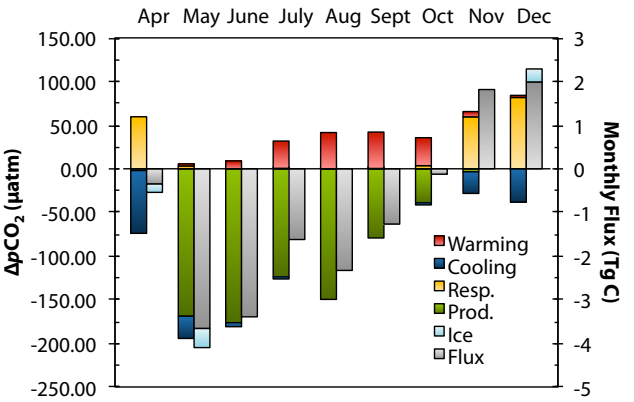

Figure 6. Area-weighted monthly average fluxes and flux drivers for the Bering Sea shelf. Fluxes are indicated in gray, while flux drivers are indicated by the color series: warming and cooling are shown in red and blue, respectively, and production and respiration are indicated in green and yellow, respectively. The calculations for these series are given in section 2. Most of the time, temperature influences directly oppose biological influences with near-equilibrium achieved in April and October. Note particularly the new observations of net shelf-wide CO_2 efflux occurring in conjunction with respiration processes during November and December. An estimate of the interpolated dampening of sea-air CO_2 fluxes by ice cover is also shown, as discussed in section 3.3.

and 34 μatm, respectively), and $F_{CO_2(aw)}$ was closest to equilibrium during that month (-0.12 Tg C month^{-1}).

Few previous observations later in the year than September exist, and the biogeochemical processes occurring during autumn and winter ("late season"; i.e., October to March) are not well understood. Earlier work has shown that respiration processes cause CO_2 accumulation in bottom waters over the shelf during the preceding summer, particularly in regions corresponding to high primary production levels in the overlying surface waters [e.g., *Mathis et al*., 2010, 2011a, 2011b; *Cross et al*., 2012; *Mathis et al*., 2014]. We observed here that biogeochemical processes substantially modified surface waters in autumn and winter. During November and December, respiration dominated variability in surface layer $F_{CO_2(aw)}$ ($+1.82$ and 2.29 Tg C month^{-1}, respectively). The contribution of stronger wind speeds is also obvious during these later months: the ratio of $F_{CO_2(aw)}$ to ΔpCO_2 was 50–65% larger than on average (not shown).

No data were available for January, February, and March. However, shelf-wide processes in April were similar to those occurring in November and December, with cooling processes and respiration acting as the dominant drivers of ΔpCO_2. An important distinction between these months was that cooling processes controlled ΔpCO_2 and $F_{CO_2(aw)}$ (-0.54 Tg C month^{-1}) during April, despite the same contribution of respiration to ΔpCO_2 ($\sim$60 μatm) as was observed to control $F_{CO_2(aw)}$ in November and December. April was the only month in which changing temperature was the dominant driver of $F_{CO_2(aw)}$, although warming nearly balanced the contribution of primary production to $F_{CO_2(aw)}$ in October.

Overall, the average F_{CO_2} value over the 9 months included in this study is -4.03 ± 12.35 mmol CO_2 m^{-2} d^{-1} (Table 3). Because the time scale of equilibration of the surface ocean with the atmosphere can be longer than the 1 month averages over which we have calculated these fluxes, we integrated this 9 month average value over 365 days to avoid overestimating the contribution of remnant fluxes that overlap between months. According to this scaling, the integrated annual flux would be -12.27 Tg C yr^{-1}. However, the missing 3 months of winter data biases the annual estimate toward the spring and summer values, and overestimates the size of an annual Bering Sea CO_2 sink.

Given the similarities between November, December, and April, where respiration and cooling dominate the shelf, it may be more reasonable to assume that January, February, and March can also be considered to operate under this winter pattern. Previous work has shown that pCO_2(sw) continues to evolve through the winter months in ice-covered environments [e.g., *Gibson and Trull*, 1999; *Shadwick et al*., 2011; *Else et al*., 2012]. In order to make a more reasonable annual estimation from the available data, we applied a linear interpolation of $F_{CO_2(aw)}$ between December and April to estimate $F_{CO_2(aw)}$ during January, February, and March. These fluxes were all positive (1.6, 0.9, and 0.2 Tg C month^{-1}, respectively), resulting in a shelf-wide annual flux of -6.6 Tg C yr^{-1}, approximately 46% lower than scaling to the 9 month average as described above. This value is similar to some previous estimates based solely on summer observations [*Codispoti et al*., 1986] and long-term modeling efforts [*Takahashi et al*., 2009].

This difference strongly highlights the importance of late-season thermodynamic and biogeochemical processes for sea-air exchange estimates for the Bering Sea and for the understanding of the Bering Sea carbon cycle. Neglecting to include positive wintertime fluxes when estimating an annual $F_{CO_2(aw)}$ value for the Bering Sea would have resulted in an almost fourfold increase in the size of the Bering Sea sink:

AGU Journal of Geophysical Research: Oceans 10.1002/2013JC009579

Table 2. Monthly Area-Weighted Sea-Air ΔpCO_2 (μatm), Biological and Thermal Drivers of ΔpCO_2 (μatm), Monthly Flux Rates (mmol C m^{-2} d^{-1}), and Net Monthly Fluxes (Tg C)[a]

Parameter	Units	April	May	June	July	August	September	October	November	December
Net ΔpCO_2	μatm	−13.55 ± 50.85	−190.24 ± 73.63	−172.36 ± 71.26	−91.74 ± 65.88	−108.14 ± 65.88	−37.02 ± ± 56.43	−3.31 ± 36.43	39.19 ± 54.55	44.29 ± 45.67
$\Delta pCO_{2(aw)}$		*n = 73*	*n = 618*	*n = 499*	*n = 220*	*n = 220*	*n = 203*	*n = 249*	*n = 203*	*n = 437*
Net biology (*B*)	μatm	57.23 ± 59.45	−164.78 ± 83.03	−176.33 ± 55.52	−122.93 ± 55.52	−149.66 ± 60.88	−78.71 ± 48.89	−35.18 ± 38.03	55.54 ± 59.78	81.65 ± 35.73
$n\Delta pCO_{2(aw)}$		*n = 73*	*n = 618*	*n = 499*	*n = 499*	*n = 387*	*n = 203*	*n = 249*	*n = 203*	*n = 437*
Production	μatm	−2.05 ± 2.07	−168.93 ± 50.80	−176.33 ± 55.52	−123.82 ± 50.96	−149.65 ± 59.72	−79.28 ± 44.99	−33.97 ± 23.88	−3.48 ± 3.09	−0.02 ± 0.00
$+n\Delta pCO_{2(aw)}$		*n = 9*	*n = 571*	*n = 499*	*n = 216*	*n = 385*	*n = 196*	*n = 211*	*n = 38*	*n = 1*
Respiration	μatm	59.60 ± 48.51	3.20 ± 4.70	n/a	0.57 ± 0.48	0.00 ± 0.00	0.40 ± 0.35	3.60 ± 4.32	59.52 ± 42.27	81.69 ± 35.42
$-n\Delta pCO_{2(aw)}$		*n = 74*	*n = 47*	*n = 0*	*n = 4*	*n = 2*	*n = 7*	*n = 38*	*n = 165*	*n = 436*
Net temperature (*T*)	μatm	−71.91 ± 15.95	−25.45 ± 12.74	3.97 ± 23.37	32.35 ± 19.75	41.52 ± 12.91	41.68 ± 16.25	31.87 ± 18.22	−16.35 ± 35.95	−37.36 ± 24.28
$\Delta pCO_{2(aw)} - n\Delta pCO_{2(aw)}$		*n = 73*	*n = 618*	*n = 499*	*n = 220*	*n = 387*	*n = 203*	*n = 249*	*n = 203*	*n = 437*
Cooling	μatm	−71.91 ± 15.95	−25.47 ± 12.45	−4.62 ± 3.26	−0.02 ± 0.00	n/a	n/a	−0.19 ± 0.17	−24.74 ± 17.53	−38.09 ± 21.53
$-(\Delta pCO_{2(aw)} - n\Delta pCO_{2(aw)})$		*n = 73*	*n = 613*	*n = 275*	*n = 1*	*n = 0*	*n = 0*	*n = 7*	*n = 125*	*n = 422*
Warming	μatm	n/a	0.01 ± 0.00	9.02 ± 11.57	31.21 ± 19.55	41.52 ± 12.91	41.68 ± 16.25	32.00 ± 16.73	6.06 ± 3.27	0.50 ± 0.42
$+(\Delta pCO_{2(aw)} - n\Delta pCO_{2(aw)})$		*n = 0*	*n = 5*	*n = 224*	*n = 219*	*n = 387*	*n = 203*	*n = 242*	*n = 78*	*n = 15*
Flux	mmol C m^{-2} d^{-1}	−2.16 ± 4.45	−15.85 ± 6.86	−13.56 ± 5.78	−6.27 ± 6.64	−9.01 ± 6.13	−5.06 ± 7.57	−0.48 ± 5.42	7.26 ± 10.52	8.85 ± 8.53
$F_{CO2(aw)}$	Tg C	−0.54 ± 1.11	−4.10 ± 1.77	−3.39 ± 1.45	−1.62 ± 1.72	−2.33 ± 1.59	−1.26 ± 1.89	−0.12 ± 1.40	1.82 ± 2.63	2.29 ± 2.20
Flux ice	mmol C m^{-2} d^{-1}	−2.20 ± 3.92	−15.68 ± 6.99	n/a	n/a	n/a	n/a	n/a	n/a	8.87 ± 8.37
$F_{CO2ice(aw)}$	Tg C	−0.55 ± 0.98	−4.05 ± 1.81							2.29 ± 2.16
Flux ice interp	mmol C m^{-2} d^{-1}	−1.41 ± 0.75	−14.15 ± 2.56	n/a	n/a	n/a	n/a	n/a	n/a	7.71 ± 1.96
$F_{CO2iceinterp(aw)}$	Tg C	−0.35 ± 0.19	−3.66 ± 0.66							1.99 ± 0.51

[a]Ice-corrected flux rates and net fluxes are also included for ice-impacted months (April, May, and December).

Table 3. Annual Sea-Air CO_2 Fluxes on the Bering Sea Shelf Based on Different Types of Calculations[a]

Annual Flux	Observation Type	mmol C m^{-2} d^{-1}	Tg C yr^{-1}
Codispoti et al. [1986]	Summer Obs.	−0.66	−2.01
Takahashi et al. [2009]	Climatology	−1.2	−3.65
Walsh and Dieterle [1994][b]	Numerical Model	−11.78	−35.61
Kaltin and Anderson [2005][b]	Synthesis—North	−19.62	−59.72
Bates et al. [2011]	Spring-Summer Obs.	−22	−66.96
This Study			
$F_{CO_2(aw)}$	April to December obs.	−4.03	−12.27
$F_{CO_2(aw)}$ - ND	Spring-summer obs.	−7.48	−22.78
$F_{CO_2(aw)}$ + JFM	Annual estimate	−2.19	−6.66
$F_{CO_2(aw)ice}$ + JFM	Ice correction	−2.24	−6.81

[a]All fluxes in this table were scaled from average annual flux rates (mmol C m^{-2} d^{-1}) to 365 days and the area of the Bering Sea shelf (6.94×10^{11} m^2). Literature values for flux rates were taken from the synthesis of *Chen and Borges* [2009] and *Bates et al.* [2011], but were limited to studies describing data collected only in the southeastern Bering Sea.

[b]Note that the estimates from *Walsh and Dieterle* [1994] and *Kaltin and Anderson* [2005] were originally reported in units of mol C m^{-2} yr^{-1}.

the average $F_{CO_2(aw)}$ from April to October was −22.78 Tg C yr^{-1}. This production-season only value is similar to other annual fluxes previously reported for the Bering Sea shelf that also used primarily production season data incorporated into larger models and climatological approaches (see estimates from *Walsh and Dieterle* [1994], *Kaltin and Anderson* [2005], and *Bates et al.* [2011] in Table 3). Future measurement programs should target these important CO_2 efflux months to better refined estimates of annual exchange.

3.3. Present and Future Implications of Seasonal Ice Cover

As we discussed above, the NARR wind product generates very low wind speeds over sea ice, resulting in minimal F_{CO_2} values despite occasionally large ΔpCO_2 (Figure 5). Owing to the already low F_{CO_2} values, applying our ice-cover dampening proxy does not have much effect on the average shelf-wide fluxes during each individual month. Overall, accounting for ice resulted in $<2\%$ change in monthly $F_{CO_2(aw)}$ and a $<1\%$ change in annual $F_{CO_2(aw)}$ ($\sim$0.01 Tg). According to this parameterization, it does not appear that the ice matrix has a significant direct effect on current sea-air CO_2 fluxes in the Bering Sea. However, our measurements were not necessarily taken in proportion to the areas of open water and ice cover. A bias toward open water or under ice estimates could underestimate or overestimate the impact of ice cover, respectively.

Just as we applied an interpolation to fill missing winter data and better represent an otherwise biased annual flux estimate above, we implemented a similar interpolation to better estimate the impacts of sea ice in areas where measurements were unavailable. In order to correct for this spatial inhomogeneity, we applied our ice cover correction to our entire spatial grid populated uniformly by the monthly $F_{CO_2(aw)}$. This resulted in a much greater impact of the mechanical inhibition of ice on $F_{CO_2(aw)}$ during ice-covered months (see last row, Table 2). During maximum ice extent in April, the ice-adjusted flux ($F_{CO_2(aw)i}$) was lower than $F_{CO_2(aw)i}$ by 35%, and during ice retreat, in May, and ice advance, in December, $F_{CO_2(aw)}$ was reduced by approximately 10% (see Table 2 and Figure 6). We also populated a grid with ice cover from January, February, and March and the interpolated $F_{CO_2(aw)}$ we calculated from these months. Like in April, fluxes during these ice-rich months were reduced by 18.5%, 24%, and 29.5% respectively. The new annual flux resulting from this inhomogeneity correction is approximately −6.8 Tg C yr^{-1}, only adding only 0.2 Tg C yr^{-1} to the annual CO_2 sink as estimated using the simpler approach applied above.

In addition to this mechanical inhibition, it is important to consider that ice cover indirectly affected the CO_2 flux calculations both by lowering wind speed and by changing the balance between biological and physical drivers on ΔpCO_2. During December, cooling dampened ΔpCO_2 by approximately twice as much in the ice-covered areas of the shelf relative to the ice-free regions. In the absence of temperature forcing, B in ice-impacted areas would have been 66 μatm, compared to the observed 10 μatm. During May, $\Delta pCO_{2(aw)}$ of ice-covered areas was −179 μatm. In the absence of ice, higher piston velocities from greater wind speeds would have enhanced CO_2 influx over 15% of occupied pixels during May, and over more than half of occupied pixels during December.

Table 4. Annual CO_2 Flux and Areas of Alaskan Continental Shelves[a]

	Total Annual Flux		Total Area	
Shelf	Tg C yr^{-1}	%	km^2	%
GoA[a]	14	*45.90*	800,000	*34.90*
Bering[b]	6.8	*22.30*	694,355	*30.29*
Chukchi[c]	5	*16.39*	620,000	*27.05*
Beaufort[c]	4.7	*15.41*	178,000	*7.76*
Total AK shelves	30.5	*100*	2,292,355	*100*

[a]Area and annual flux from *Evans and Mathis* [2013].
[b]Area and annual flux from this study.
[c]Area and annual flux from *Evans et al.* [2014].

The warmer, ice-reduced scenario predicted for the Bering Sea [e.g., *Stabeno et al*., 2012a, 2012b] may have broad implications for the Bering Sea carbon cycle. Longer ice-free periods during fall and winter [*Stabeno et al*., 2012a] will be accompanied by greater piston velocities due to higher wind speeds, favoring enhanced CO_2 outgassing during these periods of high respiration. Lower volumes of ice growth and ice melt will result in a diminished sea ice CO_2 pump [*Rysgaard et al*., 2008]. Reduced ice melt volumes will also weaken stratification [*Ladd and Stabeno*, 2012], increasing the potential for vertical mixing of respired CO_2 from shelf bottom waters especially during summer and fall when respiration products from the spring bloom have accumulated. Overall warming of surface waters [*Stabeno et al*., 2012a] will increase pCO_2(sw), favoring periods of stronger CO_2 efflux in open-water areas during November to April and weaker CO_2 influx from May to October. Early ice retreat may change the timing and lower the overall magnitude of the spring bloom [*Sigler et al*., 2014]. Together, these effects should act in concert to diminish the size of the Bering Sea CO_2 sink. However, the largest single biogeochemical driver of CO_2 exchange in the Bering Sea is primary productivity. Although predictions of changes in bulk primary production are difficult to make [e.g., *Moran et al*., 2012; *Hunt et al*., 2011] and would be difficult to identify due to large interannual variability [*Lomas et al*., 2012], it is possible that increased rates and volumes of primary production could also result from increased light penetration and enhanced nutrient renewal. In a reduced stratification scenario, this could offset periods of potentially stronger outgassing.

3.4. CO_2 Invasion on Alaskan Coastal Shelves

The magnitude of the newly observed late-season CO_2 efflux we have described here may also provide new insights into the Pacific Arctic carbon cycle. Nearly 65% of average monthly CO_2 influx (-22.78 Tg C yr^{-1}) is balanced by average late-season efflux processes (15.97 Tg C yr^{-1}), including our interpolation of effluxes for January to March. This efflux not only reduces the overall size of the annual Bering Sea sink for CO_2 but also reduces the amount of carbon that is exported from the Bering Sea to the Chukchi Sea.

Given the vast spatial extent and the high rates of primary production typical of the Bering Sea shelf, it is often assumed that the region must be a strong sink for atmospheric CO_2 [*Bates et al*., 2011]. We have shown here that late-season outgassing partially counteracts spring and summer CO_2 influxes, shrinking the size of the potential sink. The resulting total CO_2 influx is stronger than in the Chukchi and Beaufort seas, and combined with its large size the Bering Sea accounts for over 20% of the total CO_2 invasion occurring on the Alaskan Coastal shelves (see Table 4).

Similar methods to those employed here were used to generate the net Gulf of Alaska CO_2 flux [*Evans and Mathis*, 2013] and Chukchi and Beaufort Sea fluxes [*Evans et al*., 2014]. At present, the Gulf of Alaska represents nearly half of the CO_2 sink for the Alaskan coast, despite comprising only 35% of the area. This represents a significant source of carbon for the Bering Sea. The impact of this transport would be difficult to constrain due to limited transport studies between the two basins. However, the fluxes themselves may be disproportionate, owing to calculation and scaling differences between these analyses. A better comparison of each of the shelves and the calculation of a net Alaskan Shelf CO_2 sink would require a uniform synthesis of direct measurements, over matching time and space scales sufficient to resolve regional variability. While this is difficult to achieve using solely direct measurements, a synthetic approach that enlists satellite data [i.e., *Hales et al*., 2012] blended with direct measurements may hold promise as an avenue for generating basin-scale CO_2 flux products.

3.5. Improvements and Future Directions

The synthesis in this study represents three significant advances in the understanding of annual sea-air CO_2 fluxes in the Bering Sea: (1) we have compiled over 45,000 measurements to provide the highest spatial and temporal resolution for these calculations; (2) provided the first observation of autumn and winter effluxes

and the magnitude of their contribution on the annual scale; (3) analyzed the physical and biological processes responsible for determining the magnitude and direction of the sea-air CO_2 fluxes. Despite this progress, there remain many uncertainties with regards to sea-air CO_2 exchange in the Bering Sea.

In order to estimate the biogeochemical drivers on F_{CO_2} we here assumed that all variation in npCO_2(sw) nΔpCO_2(sw) were the result of biological modification. However, other minor processes like vertical/lateral water mass mixing and the time evolution of CO_2 flux can impact npCO_2(sw) by altering the buffering capacity [e.g., *Rysgaard et al*., 2009; *Yamamoto-Kawai et al*., 2009; *Evans et al*., 2014b] or total concentration of CO_2 in surface waters [e.g., *Mathis et al*., 2012].

Using the observational data collected during the BEST project included in this analysis, we can use the ratio of TA:DIC as a proxy for buffering capacity. Both spatially and seasonally, the variation in this ratio is large (as high as 0.2), indicating that the impact on npCO_2(sw) may also be significant [*Evans et al*., 2014b]. However, the large variability in TA:DIC in these data sets is poorly correlated with changes in salinity and TA, and nonconservative changes in DIC can account for 90% of the variability in this ratio. Relative to biological modification, the contribution of water mass mixing to variation in buffering capacity is small. While mixing processes are likely minor contributors to changes in buffering capacity, lateral and vertical advection can change nΔpCO_2(sw) by increasing or decreasing CO_2 concentrations in surface waters. Insofar as these changes are related to biological modification, as when respiration-impacted waters are mixed into the surface layer [*Mathis et al*., 2010, 2011a, 2011b; *Cross et al*., 2012], this does not represent a significant source of error to our biological term. The impact of lateral advection of new water masses is also minimal. Previous work has shown that the Yukon River can contribute as much as 1.27 Tg C yr^{-1} [*Cross et al*., 2014], which is small relative to estimates of net community production ($\sim$97 Tg C yr^{-1}) [*Mathis et al*., 2011a*; Cross et al*., 2012, 2014]. The small volume of sea ice melt and brine contributed to this area likely is also likely small on a relative scale.

The time evolution of gas exchange both changes the concentration of CO_2 in surface waters and selectively changes CO_2 concentrations relative to alkalinity. Estimating the error associated with the time evolution of pCO_2(sw) is complicated due to unknown variability in the mixed layer depth, short-term variability in the rate of gas exchange, and an unknown "time zero" for the evolution of pCO_2(sw) in a water parcel for a given month. N, the number of measurements within each pixel for a given month, has a wide range, and can be used as a metric of "confidence" in our monthly pixel averages. In months and areas with more heavily occupied pixels (such as the north-south transit route between the Aleutian Islands and Bering Strait), confidence that our averages are not biased toward a particular scenario for the time evolution of pCO_2(sw) is high. Months with very low values for N instill less confidence, and these are areas that should be targeted for future sample collection (including the unoccupied months of January, February, and March; months of April and July, where pixel were sparsely populated; and over the northwestern shelf, where occupations have been infrequent).

Our choice of wind product also heavily impacts this analysis. NARR represents the best choice of wind product presently available for the Bering Sea for a number of reasons, as we outlined above. However, despite the resolution, coverage, and accuracy advantages of NARR, the best confirmation of this product would be comparison with observational wind records in the Bering Sea. Although NARR has been shown to correlate well with wind products in the Chukchi and Beaufort seas [e.g., *Pickart et al*., 2011], corresponding records and confirmation for the Bering Sea are unfortunately not available. While we are confident that the qualitative variability in the NARR climatology is sound, confirmation of quantitative variability would be better. At present, the best scaling available for the quantitative wind speeds in NARR is the SCOW product. SCOW compares well to weather records in the Gulf of Alaska [*Evans and Mathis*, 2013], and the quantitative values between NARR and SCOW are very similar (see Figure S1 in supporting information). Because NARR includes wind speeds from the northern shelf, where winds are typically lower, monthly average wind speeds from NARR are typically lower than in SCOW. If NARR modeled winds are slower than observed winds, the fluxes we have calculated here represent conservative estimates.

Another challenge in calculating fluxes for the Bering Sea is the naturally small-scale spatial and temporal variability of biogeochemical processes. Many studies have suggested the definition of as many as 16 distinct subregional spatial domains based on physical [*Coachman*, 1986; *Kachel et al*., 2002], biogeochemical [*Mathis et al*., 2010; *Cross et al*., 2012, 2014], and ecosystem-level variability [*Ortiz et al*., 2012; *Harvey and*

Sigler, 2013; *Baker and Hollowed*, 2014]. Additionally, interannual variability can be quite large [*Stabeno et al*., 2001; *Danielson et al*., 2011; *Lomas et al*., 2012]. Although this study includes more than 45,000 measurements, most grid cells are occupied with <15 observations, usually all within a single year. Because our sampling resolution is low relative to the scale of variability in the Bering Sea, small-scale patchiness, or interannual anomalies occurring in some grid cells, may have been overweighted.

This challenge may be easily resolved in the future; here the deployment of several underway systems on frequently used vessels has provided greater temporal coverage than has previously been available. However, these high-resolution underway systems are tethered to ships, which represent both technical and financial restrictions. Technological advances in mobile autonomous platforms may provide significant advantages in the future, such as operating in extreme environments (e.g., near the ice edge; broadly reviewed by *Wynn et al*. [2014]); cost-effective mapping and monitoring on large spatiotemporal scales [*Mellinger et al*., 2012; *Doney et al*., 2012]; and rapid deployments [*Hagen et al*., 2008]. Operational capabilities continue to develop, with promising recent advances made in tracking advective features [*Das et al*., 2012; *Brink and Pebesma*, 2013]. The best near-term opportunities for covering large spatial areas should capitalize on these type of deployments, blending not only satellite and focused ship-based observations [e.g., *Evans et al*., 2013; *Hales et al*., 2012], but including fixed autonomous and mobile autonomous sensing as well [e.g., *Evans et al*., 2013].

4. Conclusions

A synthesis of spatially resolved underway and discrete observational data for 2008–2012 provided a unique opportunity to assess autumn and winter sea-air CO_2 fluxes and consider the impact of physical and biological processes on sea-air CO_2 exchange over the Bering Sea shelf. While some influence of changing temperature on fluxes was observed, biological processes dominated most variability in sea-air exchange. In particular, late-season respiration was observed to have a substantial impact on annual CO_2 fluxes, balancing more than half of the potential annual CO_2 sink. Overall, we estimate that the size of the Bering Sea sink is approximately 6.8 Tg C yr^{-1}.

Ice cover was observed to impact CO_2 fluxes by limiting wind speed through enhanced surface roughness, and by contributing to cooler temperatures over the shelf. Because these two parameters limited potential CO_2 fluxes in ice-covered areas, a first-order estimation of the mechanical inhibition of gas exchange by the ice matrix did not have a substantial impact on net fluxes. The inhibition of efflux that occurs during autumn and winter may enhance the undersaturated conditions for calcium carbonate minerals previously observed in this region.

A comparison to other Pacific Arctic shelves indicates that other shallow shelves might experience a similar late-season outgassing resulting from net respiration. Quantification of winter outgassing could therefore reduce the overall size of the Pacific Arctic sink for CO_2 by a substantial amount, even when some inhibition of fluxes by ice cover occurs. If future warming causes significant ice losses over the next several decades, inhibition of respiration-driven CO_2 outgassing may decrease, reducing the magnitude of the Bering Sea sink and causing a significant slowing of carbon uptake in the Pacific Arctic region.

Acknowledgments
The authors thank the officers and crew of USCGC *Healy*, R/V *Knorr*, and NOAA ships *Miller Freeman* and *Oscar Dyson* for their work in supporting our science during multiple cruises. We also thank Tim Newberger (University of Colorado) and Scott Hiller (SIO) for providing engineering support for pCO_2 measurements and our colleagues from the NSIDC, LDEO, NOAA Eco-FOCI group, and the Bering Sea Project. This manuscript is BEST-BSIERP contribution 146 and PMEL contribution 3915. This synthesis effort was supported by the National Science Foundation (PLR-1107997 and ARC-1107645). The pCO_2 program aboard USCGC *Healy* is supported by NOAA grant NA08OAR4320754 to T.T. All data sets used to generate the analysis performed here can be found as listed in section 2.

References

Baker, M. R., and A. B. Hollowed (2014), Delineating ecological regions in marine systems: Integrating physical structure and community composition to inform spatial management in the eastern Bering Sea, *Deep Sea Res., Part II*, doi:10.1016/j.dsr2.2014.03.001, in press.

Bates, N. R., J. T. Mathis, and M. A. Jeffries (2011), Air-sea CO_2 fluxes on the Bering Sea shelf, *Biogeosciences*, *8*, 1237–1253, doi:10.5194/bg-8-1237-2011.

Brink, J., and E. Pebesma (2013), Plume tracking with a mobile sensor based on incomplete and imprecise information, *Transactions in GIS*, *18*, 740–766, doi:10.1111/tgis.12063.

Burba, G. G., D. K. McDermitt, A. Grelle, D. J. Anderson, and L. Xu (2008), Addressing the influence of instrument surface heat exchange on the measurements of CO_2 flux from open-path gas analyzers, *Glob. Change Biol.*, *14*, 1854–1873, doi:10.1111/j.1365-2486.2008.01606.x.

Chen, C.-T. A., and A. V. Borges (2009), Reconciling opposing views on carbon cycling in the coastal ocean: Continental shelves as sinks and near-shore ecosystems as sources of atmospheric CO_2, *Deep Sea Res., Part II*, *56*(8-10), 578–590, doi:10.1016/j.dsr2.2009.01.001.

Chen, C.-T. A., A. Adreev, K.-R. Kim, and M. Yamamoto (2004), Roles of continental shelves and marginal seas in the biogeochemical cycles of the north Pacific Ocean, *J. Oceanogr.*, *60*, 17–44, doi:10.1023/B:JOCE.0000038316.56018.d4.

Coachman, L. K. (1986), Circulation, water masses, and fluxes on the southeastern Bering Sea shelf, *Cont. Shelf Res.*, *5*(1-2), 23–108, doi:10.1016/0278-4343(86)90011-7.

Codispoti, L. A., G. E. Friederich, and D. W. Hood (1986), Variability in the inorganic carbon system over the southeastern Bering Sea shelf during spring 1980 and spring-summer 1981, *Cont. Shelf Res.*, *5*(1-2), 133–160, doi:10.1016/0278-4343(86)90013-0.

Cooper, L., M. G. Sexson, J. M. Grebmeier, R. Gradinger, C. W. Mordy, and J. R. Lovvorn (2013), Linkages between sea-ice coverage, pelagic-benthic coupling, and the distribution of spectacled eiders: Observations in March 2008, 2009, and 2010, *Deep Sea Res., Part II*, *94*, 31–43, doi:10.1016/j.dsr2.2013.03.009.

Cross, J. N., J. T. Mathis, and N. R. Bates (2012), Hydrographic controls on net community production and total organic carbon distributions in the eastern Bering Sea, *Deep Sea Res., Part II*, *65–70*, 98–109, doi:10.1016/j.dsr2.2012.02.003.

Cross, J. N., J. T. Mathis, N. R. Bates, and R. H. Byrne (2013), Conservative and non-conservative variations of total alkalinity on the southeastern Bering Sea shelf, *Mar. Chem.*, *154*, 100–112, doi:10.1016/j.marchem.2013.05.012.

Cross, J. N., et al. (2014), Integrated assessment of the carbon budget in the southeastern Bering Sea, *Deep Sea Res., Part II*, doi:10.1016/j.dsr2.2014.03.003, in press.

Danielson, S., L. Eisner, T. Weingartner, and K. Aagaard (2011), Thermal and haline variability over the central Bering Sea shelf: Seasonal and interannual perspectives, *Cont. Shelf Res.*, *31*(6), 539–554, doi:10.1016/j.csr.2010.12.010.

Das, J., F. Py, T. Maughan, T. O'Reilly, M. Messié, J. Ryan, G. S. Sukjatme, and K. Rajan (2012), Coordinated sampling of dynamic oceanographic features with underwater vehicles and drifters, *Int. J. Robotics Res.*, *31*(5), 626–646, doi:10.1177/0278364912440736.

Delille, B., B. Jourdain, A. V. Borges, J.-L. Tison, and D. Delille (2007), Biogas (CO_2, O_2, dimethylsulfide) dynamics in spring Antarctic fast ice, *Limnol. Oceanogr. Methods*, *52*(4), 1367–1379, doi:10.4319/lo.2007.52.4.1367.

Dickson, A. G. (1990), Thermodynamics of the dissolution of boric acid in synthetic seawater from 274.15 to 318.15 K, *Deep Sea Res., Part A*, *37*(5), 755–766, doi:10.1016/0198-0149(90)90004-F.

Dickson, A. G., and F. J. Millero (1987), A comparison of the equilibrium constants for the dissociation of carbonic acid in seawater media, *Deep Sea Res., Part A*, *34*(10), 1733–1743, doi:10.1016/0198-0149(87)90021-5.

Dickson, A. G., C. L. Sabine, and J. R. Christian (Eds.) (2007), *Guide to Best Practices for Ocean CO_2 Measurements*, North Pac. Mar. Sci. Organ., Sydney, B. C.

Doney, S. C., et al. (2012), Climate change impacts on marine ecosystems, *Annu. Rev. Mar. Sci.*, *4*, 11–37, doi:10.1146/annurev-marine-041911-111611.

Dornblaser, M. M., and R. G. Striegl (2007), Nutrient (N, P) loads and yields at multiples scales and sub-basin types in the Yukon River basin, Alaska, *J. Geophys. Res.*, *154*, G04S57, doi:10.1029/2006JG000366.

Else, B. G. T., T. N. Papakyriakou, M. A. Granskog, and J. J. Yackel (2008), Observations of sea surface fCO_2 distributions and estimated air-sea CO_2 fluxes in the Hudson Bay region (Canada) during the open water season, *J. Geophys. Res.*, *113*, C08026, doi:10.1029/2007JC004389.

Else, B. G. T., T. N. Papakyriakou, R. J. Galley, W. M. Drennan, L. A. Miller, and H. Thomas (2011), Wintertime CO_2 fluxes in an Arctic polynya using eddy covariance: Evidence for enhanced air-sea gas transfer during ice formation, *J. Geophys. Res.*, *116*, C00G03, doi:10.1029/2010JC006760.

Else, B. G. T., T. N. Papakyriakou, R. J. Galley, A. Mucci, M. Gosselin, L. A. Miller, E. H. Shadwick, and H. Thomas (2012), Annual cycles of pCO_{2sw} in the southeastern Beaufort Sea: New understandings of air-sea CO_2 exchange in arctic polynya regions, *J. Geophys. Res.*, *117*, C00G13, doi:10.1029/2011JC007346.

Evans, W., and J. T. Mathis (2013), The Gulf of Alaska coastal ocean as an atmospheric CO_2 sink, *Cont. Shelf Res.*, *65*, 52–63, doi:10.1016/j.csr.2013.06.013.

Evans, W., J. T. Mathis, P. Winsor, H. Statcewich, and T. E. Whitledge (2013), A regression modeling approach for studying carbonate system variability in the northern Gulf of Alaska, *J. Geophys. Res.*, *118*, 1–14, doi:10.1029/2012JC008246.

Evans, W., J. T. Mathis, J. N. Cross, K. E. Frey, and N. R. Bates (2014), A synthesis of arctic coastal ocean sea-air CO_2 fluxes surrounding the Canada Basin, paper presented at 2014 Ocean Sciences Meeting, Honolulu, Hawaii.

Gibson, J. A. E., and T. W. Trull (1999), Annual cycle of fCO_2 under sea-ice and in open water in Prydz Bay, East Antarctica, *Mar. Chem.*, *66*(3–4), 187–200, doi:10.1016/S0304–4203(99)00040-7.

Hagen, P. E., N. Størkersen, B.-E. Marthinsen, G. Stein, and K. Vestgård (2008), Rapid environmental assessment with autonomous underwater vehicles—Examples from HUGIN operations, *J. Mar. Syst.*, *69*(1-2), 137–145.

Hales, B., P. G. Strutton, M. Saraceno, R. Letelier, T. Takahashi, R. A. Feely, C. Sabine, and F. Chavez (2012), Satellite-based prediction of pCO_2 in coastal waters of the eastern North Pacific, *Prog. Oceanogr.*, *103*, 1–15, doi:10.1016/j.pocean.2012.03.001.

Harvey, R. H., and M. F. Sigler (2013), An introduction to the Bering Sea Project: Volume II, *Deep Sea Res., Part II*, *94*, 2–6, doi:10.1016/j.dsr2.2013.04.023.

Ho, D. T., R. Wanninkhof, P. Schlosser, D. S. Ullman, D. Hebert, and K. F. Sullivan (2011), Toward a universal relationship between wind speed and gas exchange: Gas transfer velocities measured with $^3He/SF_6$ during the Southern Ocean Gas Exchange Experiment, *J. Geophys. Res.*, *116*, C00F04, doi:10.1029/2010JC006854.

Hunt, G. L., Jr., P. Stabeno, G. Walters, E. Sinclair, R. D. Brodeur, J. M. Napp, and N. A. Bond (2002), Climate change and control of the southeastern Bering Sea pelagic ecosystem, *Deep Sea Res., Part II*, *49*, 5821–5853, doi:10.1016/S0967-0645(02)00321-1.

Hunt, G. L., Jr., et al. (2011), Climate impacts on eastern Bering Sea foodwebs: A synthesis of new data and an assessment of the Oscillating Control Hypothesis, *ICES J. Mar. Sci.*, *68*(6), 1230–1243, doi:10.1093/icesjms/fsr036.

Kachel, N. B., G. L. Hunt Jr., S. A. Salo, J. D. Schumacher, P. J. Stabeno, and T. E. Whitledge (2002), Characteristics and variability of the inner front of the southeastern Bering Sea, *Deep Sea Res., Part II*, *49*(26), 5889–5909, doi:10.1016/S0967-0645(02)00324-7.

Kaltin, S., and L. G. Anderson (2005), Uptake of atmospheric carbon dioxide in Arctic shelf seas: Evaluation of the relative importance of processes that influence pCO_2 in water transported over the Bering-Chukchi Sea shelf, *Mar. Chem.*, *94*, 67–97, doi:10.1016/j.marchem.2004.07.010.

Ladd, C., and P. J. Stabeno (2012), Stratification on the eastern Bering Sea shelf revisited, *Deep Sea Res., Part II*, *65-70*, 72–83, doi:10.1016/j.dsr2.2012.02.009.

Landwehr, S., S. D. Miller, M. J. Smith, E. S. Saltzman, and B. Ward (2014), Analysis of PKT correction for direct CO_2 flux measurements over the ocean, *Atmos. Chem. Phys.*, *14*(7), 3361–3372, doi:10.5194/acp-14-3361-2014.

Lauvset, S. K., W. R. McGillis, L. Bariteau, C. W. Fairall, T. Johannessen, A. Olsen, and C. J. Zappa (2011), Direct measurements of CO_2 flux in the Greenland Sea, *Geophys. Res. Lett.*, *38*, L12603, doi:10.1029/2011GL047722.

Lewis, E. R., and D. W. R. Wallace (1998), Program developed for CO_2 system calculations, *Rep. BNL-61827*, U.S. Dep. of Energy, Oak Ridge Natl. Lab., Carbon Dioxide Inf. Anal. Cent., Oak Ridge, Tenn.

Lomas, M. W., S. B. Moran, J. R. Casey, D. W. Bell, M. Tiahlo, J. Whitefield, R. P. Kelly, J. T. Mathis, and E. D. Cokelet (2012), Spatial and seasonal variability of primary production on the Eastern Bering Sea shelf, *Deep Sea Res., Part II*, *65-70*, 126–140, doi:10.1016/j.dsr2.2012.02.010.

Loose, B., W. R. McGillis, D. Perovich, C. J. Zappa, and P. Schlosser (2014), A parameter model of gas exchange for the seasonal ice zone, *Ocean Sci.*, *10*, 17–28, doi:10.5194/os-10-17-2014.

Mathis, J. T., J. N. Cross, N. R. Bates, S. B. Moran, M. W. Lomas, C. W. Mordy, and P. J. Stabeno (2010), Seasonal distribution of dissolved inorganic carbon and net community production on the Bering Sea shelf, *Biogeosciences*, *7*, 1769–1787, doi:10.5194/bgd-7-251-2010.

Mathis, J. T., J. N. Cross, and N. R. Bates (2011a), Coupling primary production and terrestrial runoff to ocean acidification and carbonate mineral suppression in the eastern Bering Sea, *J. Geophys. Res.*, *116*, C02030, doi:10.1029/2010JC006453.

Mathis, J. T., J. N. Cross, and N. R. Bates (2011b), The role of ocean acidification in systemic carbon mineral suppression in the Bering Sea, *Geophys. Res. Lett.*, *38*, L19602, doi:10.1029/2011GL048884.

Mathis, J. T., J. N. Cross, N. Monacci, R. A. Feely, and P. J. Stabeno (2014), Evidence of prolonged aragonite undersaturations in the bottom waters of the southern Bering Sea shelf from autonomous sensors, *Deep Sea Res., Part II*, doi:10.1016/j.dsr2.2013.07.019, in press.

Mathis, J. T., et al. (2012), Storm-induced upwelling of high pCO_2 waters onto the continental shelf of the western Arctic Ocean and implications for carbonate mineral saturation states, *Geophys. Res. Lett.*, *29*, L07606, doi:10.1029/2012GL051574.

Mehrbach, C., C. H. Culberson, J. E. Hawley, and R. M. Pytkowicz (1973), Measurement of the apparent dissociation constants of carbonic acid in seawater at atmospheric pressure, *Limnol. Oceanogr.*, *18*(6), 897–907, doi:10.4319/lo.1973.18.6.0897.

Mellinger, D. K., H. Klinck, N. M. Bogue, J. Luby, H. Matsumoto, and R. Stelzer (2012), Gliders, floats, and robot sailboats: Autonomous platforms for marine mammal research, *J. Acoust. Soc. Am.*, *131*, 3493, doi:10.1121/1.4709197.

Mesinger, F., et al. (2006), North American regional reanalysis, *Bull. Am. Meteorol. Soc.*, *87*, 343–360, doi:10.1175/BAMS-87-3-343.

Miller, L. A., T. N. Papakyriakou, R. E. Collins, J. W. Deming, J. K. Ehn, R. W. Macdonald, A. Mucci, O. Owens, M. Raudsepp, and N. Sutherland (2011), Carbon dynamics in sea ice: A winter flux time series, *J. Geophys. Res.*, *116*, C02028, doi:10.1029/2009JC006058.

Moran, S. B., M. W. Lomas, R. P. Kelly, R. Gradinger, K. Iken, and J. T. Mathis (2012), Seasonal succession of net primary productivity, particulate organic carbon export, and autotrophic community composition in the eastern Bering Sea, *Deep Sea Res., Part II*, *65-70*, 84–97, doi:10.1016/j.dsr2.2012.02.011.

Mucci, A., B. Lansard, L. A. Miller, and T. N. Papakyriakou (2010), CO_2 fluxes across the air-sea interface in the southeastern Beaufort Sea: Ice-free period, *J. Geophys. Res.*, *115*, C04003, doi:10.1029/2009JC005330.

Nomura, D., H. Eicken, R. Gradinger, and K. Shirasawa (2010), Rapid physically driven inversion of the air-sea ice CO_2 flux in the seasonal landfast ice off Barrow, Alaska after onset of surface melt, *Cont. Shelf Res.*, *30*, 1998–2004, doi:10.1016/j.csr.2010.09.014.

Ortiz, I., F. Wiese, and A. Grieg (2012), Marine Regions Boundary Data for the Bering Sea Shelf and Slope, UCAR/NCAR Earth Observing Lab., Boulder, Colo., doi:10.5065/D6DF6P6C. [Available at http://data.eol.ucar.edu/codiac/dss/id=245.B99-001.]

Ono, K., A. Miyata, and T. Yamada (2008), Apparent downward CO_2 flux observed with open-path eddy covariance over a non-vegetated surface, *Theor. Appl. Climatol.*, *92*(3), 195–208, doi:10.1007/s00704-007-0323-3.

Pickart R. S., M. A. Spall, G. W. K. Moore, T. J. Weingartner, R. A. Woodgate, K. Aagaard, and K. Shimada (2011), Upwelling in the Alaskan Beaufort Sea: Atmospheric forcing and local versus non-local response. *Progress in Oceanography*, *88*(1-4), 78–110, doi:10.1016/j.pocean.2010.11.005.

Prytherch, J., M. J. Yelland, R. W. Pascal, B. I. Moat, I. Skjelvan, and C. C. Neill (2010), Direct measurements of the CO_2 flux over the ocean: Development of a novel method, *Geophys. Res. Lett.*, *37*(3), L03607, doi:10.1029/2009GL041482.

Robbins, L., M. Hansen, J. Kleypas, and S. C. Meylan (2010), CO2Calc—A user-friendly seawater carbon calculator for Windows, Mac OS X, and iOS (iPhone), U.S. Geol. Surv. Open File Rep., *2010-1280*, 17 p.

Rutgers van der Loeff, M. M., N. Cassar, M. Nicolaus, B. Rabe, and I. Stimac (2014), The influence of sea ice cover on air-sea gas exchange estimated with radon-222 profiles, *J. Geophys. Res. Oceans*, *119*, 2735–2751, doi:10.1002/2013JC009321.

Rysgaard, S., J. Bendtsen, L. T. Pedersen, H. Ramløv, and R. N. Glud (2009), Increased CO_2 uptake due to sea ice growth and decay in the Nordic Seas, *J. Geophys. Res.*, *114*, C09011, doi:10.1029/2008JC005088.

Rysgaard, S., J. Bendtsen, B. Delille, G. S. Dieckmann, R. N. Glud, H. Kennedy, J. Mortensen, S. Papadimitriou, D. N. Thomas, and J.-L. Tison (2011), Sea ice contribution to the air-sea CO_2 exchange in the Arctic and Southern Oceans, *Tellus, Ser. B*, *63*, 823–830, doi:10.1111/j.1600-0889.2011.00571.x.

Semiletov, I., A. Makshtas, and S.-I. Akasofu (2004), Atmospheric CO_2 balance: The role of Arctic sea ice, *Geophys. Res. Lett.*, *31*, L05121, doi:10.1029/2003GL017996.

Semiletov, I. P. (1999), Aquatic sources and sinks of CO_2 and CH_4 in the polar regions, *J. Atmos. Sci.*, *56*, 286–306, doi:10.1175/1520-0469(1999)056<0286:ASASOC>2.0.CO;2.

Shadwick, E. H., H. Thomas, Y. Gratton, D. Leong, S. A. Moore, T. Papakyriakou, and E. E. F. Prowe (2011), Export of Pacific carbon through the Arctic Archipelago to the North Atlantic, *Cont. Shelf Res.*, *31*, 806–816, doi:10.1016/j.csr.2011.01.014.

Sigler, M. F., P. J. Stabeno, L. B. Eisner, J. M. Napp, and F. J. Mueter (2014), Spring and fall subarctic ecosystem, the eastern Bering Sea, during 1995–2011, *Deep Sea Res., Part II*, doi:10.1016/j.dsr2.2013.12.007, in press.

Stabeno, P., J. Napp, C. Mordy, and T. Whitledge (2010), Factors influencing physical structure and lower trophic levels of the eastern Bering Sea shelf in 2005: Sea ice, tides and winds, *Prog. Oceanogr.*, *85*(3-4), 180–196, doi:10.1016/j.pocean.2010.02.010.

Stabeno, P. J., N. A. Bond, N. B. Kachel, S. A. Salo, and J. D. Schumacher (2001), On the temporal variability of the physical environment over the south-eastern Bering Sea, *Fish. Oceanogr.*, *10*(1), 81–98, doi:10.1046/j.1365-2419.2001.00157.x.

Stabeno, P. J., N. B. Kachel, M. Sullivan, and T. E. Whitledge (2002), Variability of physical and chemical characteristics along the 70-m isobath of the southeastern Bering Sea, *Deep Sea Res., Part II*, *49*, 5931–5943, doi:10.1016/S0967-0645(02)00327-2.

Stabeno, P. J., E. V. Farley Jr., N. B. Kachel, S. Moore, C. W. Mordy, J. M. Napp, J. E. Overland, A. I. Pinchuk, and M. F. Sigler (2012a), A comparison of the physics of the northern and southern shelves of the eastern Bering Sea and some implications for the ecosystem, *Deep Sea Res., Part II*, *65-70*, 14–20, doi:10.1016/j.dsr2.2012.02.019.

Stabeno, P. J., N. B. Kachel, S. E. Moore, J. M. Napp, M. Sigler, A. Yamaguchi, and A. N. Zerbini (2012b), Comparison of warm and cold years on the southeastern Bering Sea shelf and some implications for the ecosystem, *Deep Sea Res., Part II*, *65-70*, 31–45, doi:10.1016/j.dsr2.2012.02.020.

Takahashi, T., et al. (2002), Global sea-air CO_2 flux based on climatological surface ocean pCO_2, and seasonal biological and temperature effects, *Deep Sea Res., Part II*, *49*, 1601–1622, doi:10.1016/S0967-0645(02)00003-6.

Takahashi, T., et al. (2009), Climatological mean and decadal change in surface ocean pCO_2, and net sea-air CO_2 flux over the global oceans, *Deep Sea Res., Part II*, *56*(8-10), 554–577, doi:10.1016/j.dsr2.2008.12.009.

Takahashi, T., S. C. Sutherland, and A. Kozyr (2014), Global ocean surface water partial pressure of CO_2 database: Measurements performed during 1957 – 2013 (Version 2013), ORNL/CDIAC-160, NDP-088(V2013), Carbon Dioxide Inf. Anal. Cent., Oak Ridge Natl. Lab., U.S. Dep. of Energy, Oak Ridge, Tenn.

Vancoppenolle, M., et al. (2013), Role of sea ice in global biogeochemical cycles: Emerging views and challenges, *Quat. Sci. Rev.*, *79*, 207–230, doi:10.1016/j.quascirev.2013.04.011.

Walsh, J., and D. W. Dieterle (1994), CO_2 cycling in the coastal ocean. I—A numerical analysis of the southeastern Bering Sea with applications to the Chukchi Sea and the northern Gulf of Mexico, *Prog. Oceanogr.*, *34*, 335–392, doi:10.1016/0079–6611(94)90019-1.

Walsh, J., and C. Johnson (1979), An analysis of Arctic sea ice fluctuations, 1953-77, *J. Phys. Oceanogr.*, *9*(3), 580–591, doi:10.1175/1520-0485(1979)009<0580:AAOASI>2.0.CO;2.

Weiss, R. F. (1974), Carbon dioxide in water and seawater: The solubility of a non-ideal gas, *Mar. Chem.*, *2*, 203–215, doi:10.1016/0304-4203(74)90015-2.

Wynn, R. B., et al. (2014), Autonomous Underwater Vehicles (AUVs): Their past, present, and future contributions to the advancement of marine geoscience, *Mar. Geol.*, *352*, 451–468, doi:10.1016/j.margeo.2014.03.012.

Yamamoto-Kawai, M., F. McLaughlin, E. C. Carmack, S. Nishino, and K. Shimada (2009), Aragonite undersaturation in the Arctic Ocean: Effects of ocean acidification and sea ice melt, *Science*, *326*(5956), 1098–1100.

Zeebe, R., and D. Wolf-Gladrow (2001), *CO_2 in Seawater: Equilibrium, Kinetics, Isotopes*, 346 pp., Elsevier Sci., Amsterdam.